The effect of nasal shape on the thermal conditioning of inhaled air
Using clinical tomographic data to build a large-scale statistical shape model

Keustermans, William; Huysmans, Toon; Schmelzer, Bert; Sijbers, Jan; Dirckx, J.J.

Citation (APA)

Important note
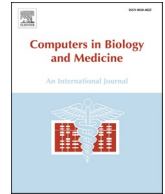To cite this publication, please use the final published version (if applicable).
Please check the document version above.

The effect of nasal shape on the thermal conditioning of inhaled air: Using clinical tomographic data to build a large-scale statistical shape model

William Keustermans [a,*], Toon Huysmans [b], Bert Schmelzer [c], Jan Sijbers [d], Joris JJ. Dirckx [a]

[a] Physics Department, University of Antwerp, Laboratory of Biophysics and Biomedical Physics, Groenenborgerlaan 171, 2020, Antwerp, Belgium
[b] Section on Applied Ergonomics and Design, Faculty of Industrial Design Engineering, Delft University of Technology, Landbergstraat 15, 2628, CE Delft, Netherlands
[c] ENT Department, ZNA Middelheim Hospital, Lindendreef 1, 2020, Antwerp, Belgium
[d] Physics Department, University of Antwerp, Imec-Vision Lab, Universiteitsplein 1, 2610, Antwerp, Belgium

ABSTRACT

In this paper, we investigate the heating function of the nasal cavity qualitatively, using a high-quality, large-scale statistical shape model. This model consists of a symmetrical and an asymmetrical part and provides a new and unique way of examining changes in nasal heating function resulting from natural variations in nasal shape (as obtained from 100 clinical CT scans). Data collected from patients suffering from different nasal or sinus-related complaints are included. Parameterized models allow us to investigate the effect of continuous deviations in shape from the mean nasal cavity. This approach also enables us to avoid many of the compounded effects on flow and heat exchange, which one would encounter when comparing different patient-specific models. The effects of global size, size-related features, and turbinate size are investigated using the symmetrical shape model. The asymmetrical model is used to investigate different types of septal deviation using Mladina's classification. The qualitative results are discussed and compared with findings from the existing literature.

1. Introduction

The nose is an important organ in the human body, performing multiple functions such as respiration, humidification, olfaction, filtration, and air conditioning. People suffering from nasal function impairment can experience a reduced quality of life [1]. All nasal functions have been extensively studied for healthy and pathological noses (see, for example, [2–4]. Due to the complex structure of the nasal cavity, detailed in vivo measurements are unfeasible and numerical simulations based on computational fluid dynamics (CFD) have become standard techniques in research into the nasal cavity [5]. Over the last three decades, CFD has been increasingly used to predict airflow through the nasal cavity based on three-dimensional models derived from medical images [2,7–13].

Past research was focused mainly on nasal resistance to airflow and on the minimal cross-sectional area inside the nasal cavity as a measure of nasal obstruction [14]. However, CFD can also be linked to the physical law describing heat transfer. More recently, it was found that subjective complaints from patients may be more related to the activation of a temperature-sensitive mechanism by the inspired air than the

exerted effort during inhalation [14–16].

Other work on nasal heat transfer investigates the relationship between nasal shape and climate [17,18]. For example, in anthropological studies, a distinction is made between broad and narrow external noses, and researchers have investigated how these differences are geographically related [17–20].

Various numerical simulations have been run specifically to study heat transport inside the nasal cavity. Examples of such simulations are studies into noses after turbinate surgery [21], healthy noses [5,22–24], noses with septal perforations [25], and patients suffering from atrophic rhinitis [2].

The conditioning of inhaled air is an essential nasal function. Situated in the deepest parts of the lungs are sensitive regions called the alveolar cavities [26]. The regulation of the temperature of inspired air is vital to protect the delicate mucosal tissue of the lungs [17]. Therefore, it is believed that the nasal cavity has evolved into a natural and efficient heat exchanger [27–30]. However, of all the functions of the nasal cavity, the heating function is the one which is the least understood. When we investigate the heating capacity of the nasal cavity, it is crucial that we start from the alveolar condition. The alveolar condition
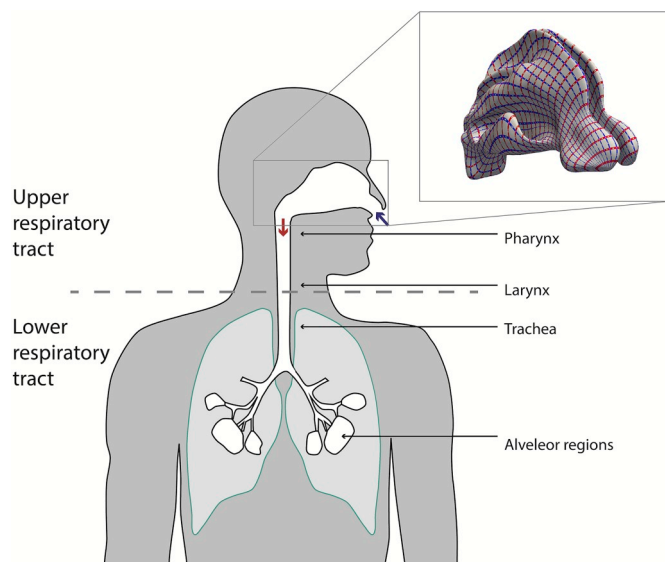
states that inhaled air should be conditioned to the core body temperature of 37 °C and to 100% relative humidity when it reaches the alveoli (Fig. 1) to ensure undisturbed alveolar gas exchange in the lungs [31]. When we consider how healthy airways function, the alveolar condition places a substantial restriction on the air temperature entering the alveoli cavities. The outside air reaches this temperature by passing through parts of the upper airway (nasal cavity, pharynx) and parts of the lower airway (larynx, trachea, bronchus), before eventually entering the alveoli. Each region contributes to the conditioning of the air, and it is the restriction on the first part of the airway tract, the nasal cavity, that will be of interest in this paper and will be used below as the basis for interpreting the results. In the literature, variation exists on the reported air temperature in the nasopharyngeal region, with numbers depending on the temperature of the ambient air, and ranging from 25 °C to 37.7 °C [24,31–37]. Other scholars express the contribution of the nasal cavity in relative numbers and report that the nasal cavity is responsible for 75%–92% of the temperature increase over the complete airway tract [24,38].

Nowadays, most of the numerical simulations of the heating function of the nasal cavity are limited to case studies, in which only one or a handful of nasal geometries are used, not accounting for localized geometry manipulations, such as virtual turbinate resections, virtual septoplasty or radical sinus surgery [39–42]. Exceptions are, for example, [15,16]; who investigated 10 and 22 nasal geometries, respectively.

In the present paper, we adopt a different approach and investigate the nasal heating function, combining computational fluid dynamics (CFD) with a large-scale statistical shape model (SSM) of the nasal cavity. This approach allows us to take a different and unique look at the relationship between nasal function and shape. In addition, the approach allows us to apply incremental and continuous anatomical changes to nasal shape based on the natural variation in real clinical tomographic data. By dividing the general model into a symmetrical and an asymmetrical shape model, we are able to analyze the effect of symmetry or the lack thereof continuously. For example, the symmetrical model can be used to study the effect of variations in the size of different types of conchae in the absence of asymmetry. The asymmetrical shape model can be used to examine the variety and degree of septum deviation. The presence of asymmetrical variations in the

investigation of shape features unrelated to asymmetry can obscure results because of compounding effects. In Section 2, the different techniques used in this paper are provided. In Section 3, the results are presented. In Section 4, we discuss our findings.

2. Methods

2.1. Statistical shape modeling

Triangular surface data extracted from 100 computed tomography (CT) scans were used to create a statistical shape model (SSM) of the human nasal cavity. The data came from 100 patients, suffering from various nasal or sinus-related complaints.

Each scan was subjected to a segmentation procedure, resulting in a collection of 100 geometric surface models. Manual grayscale thresholding was applied to distinguish between the nasal passages and other regions (e.g., soft tissue or bone). The nasal cavities and sinuses were separated manually by a single operator to avoid inter-operator-generated variations in the segmentation files. All nasal cavities were cut off posteriorly using a plane at a fixed anatomical position. If this had not been done, differences in the field of view between different scans would have resulted in substantial, unnatural variation in nasal geometry. Subsequently, all holes in the segmentation files were filled. This operation is required by the correspondence procedure discussed below. For all segmentations, the software program Amira v6.0.1 (FEI, Hillsboro, OR, USA) was used.

Subsequently, the Marching Cubes Algorithm [43] was used to generate a triangulated surface geometry for each segmentation file, after which the surface was smoothed. The asymmetrical features in a nose are not bound to one direction. For example, both left and right nasal septum deviations exist. Consequently, it is in general a good approach to apply a mirror operation on the training data collected from segmentations. The training set was doubled in size using the mirror filter in Paraview v5.4.0 (Kitware inc., NY, USA).

A surface correspondence between the different nasal geometries has to exist to be able to build an SSM: the number of triangles and vertices of each surface have to be equal (so that a one-to-one map between the training surfaces exists) and corresponding vertices of the training surface have to be at the same anatomical locations. To enable this, a modified version of the correspondence method developed by Ref. [44] was used. This method is based on the cylindrical parameterization of each surface. Consequently, all surfaces had to be free of holes and handles (i.e., they had to have a topology genus-0). In terms of compactness, the procedure leads to an optimal parameterization for each shape, which is used to generate a vertex correspondence for the training set. This step results in a training set, in which each shape is represented by a fixed number of landmarks. Across the training set, these landmarks are at corresponding anatomical locations and are uniformly distributed over the surface of the average nasal geometry.

From the set of corresponded surfaces, we constructed an SSM of the human nasal cavity by applying principal component analysis (PCA) to the 200 corresponded triangular surfaces. A nasal shape was considered independent of orientation and position. Because the SSM also considers scaling of the nasal cavity, some would refer to nasal 'form' instead of 'shape' since, strictly speaking, scaling is disregarded by shape. However, to keep the analogy with the term 'statistical shape modeling', we chose to refer consistently to shape throughout this paper, although we took into account scaling in our analysis.

Procrustes analysis, as an iterative process, was used to determine the optimal poses. To initialize the procedure, a shape from the set of training shapes was chosen as a reference shape in the first iteration, and the entire collection of noses was aligned with this shape. From the second iteration onward, the average nasal shape calculated in the previous iteration was used as a reference. After PCA, a symmetrical average nasal shape and an orthogonal set of eigenvectors were obtained. The set of eigenvectors describes the shape variations present in

Fig. 1. Overview of the human respiratory tract. Cold air is inhaled and consecutively warmed by the different parts of the airways before finally entering the alveolar cavities. The inset shows the nasal cavity, where the red and blue lines reveal the (u,v) coordinates of the map to the cylinder. The red lines are at constant v (around the cylinder) and the blue lines at constant u (along the cylinder).

the training set. A general nasal shape can be defined as the sum of the average nasal cavity and a linear combination of these shape variations. Some of the eigenvectors will explain only a small fraction of the total variation, so that the dimensionality of the shape space can be reduced. Therefore, a shape model provides a compact way of representing nasal shape variation (Fig. 2).

The statistical shape model contains both symmetrical and asymmetrical shape variations. Subsequently, a symmetry–asymmetry analysis was performed, in which we separated the shape variation into symmetrical and asymmetrical nasal variations. We created symmetrical versions of each nose to perform this analysis. In so doing, we were able to quantify the asymmetry for each shape and to model the asymmetry for the training population.

Below, the process of generating symmetrical noses is discussed. First, the mean nasal cavity was mirrored and non-rigidly registered to the original mean to obtain a correspondence between both shapes. Then, a mirrored version of each nose in the population was generated using the correspondence with the mirrored mean nose. Next, the original and mirrored versions of each nose were optimally aligned in the least-squares sense. Finally, a symmetrical nose was calculated as the point-wise average of the aligned original and mirrored noses. A symmetrical statistical shape model was built by applying PCA to the symmetrical noses. The resulting model is shown in Fig. 3.

It is also possible to analyze nasal asymmetry in the population. To this end, the difference vectors between the original and mirrored nasal shapes were calculated for each nose. Subsequently, PCA was applied to the difference vector fields to obtain a statistical model of nasal asymmetry. The asymmetrical shape components are visualized in Fig. 4. Both the symmetrical and the asymmetrical shape models are useful for further investigation by means of computational fluid dynamics (CFD).

As the last step, the shapes were divided into three parts. These parts can be used later on, during the analysis of the flow dynamics, to define regions, and to set boundary conditions (BCs) on these regions. The three parts distinguished are (1) the nostrils as inlet conditions, (2) the throat as outlet condition, and (3) the wall of the nasal cavity. These regions were defined only once, based on the mean nose. Because of existing correspondence, the parts are automatically defined for all shapes produced by the shape models and can be extracted in an automated manner.
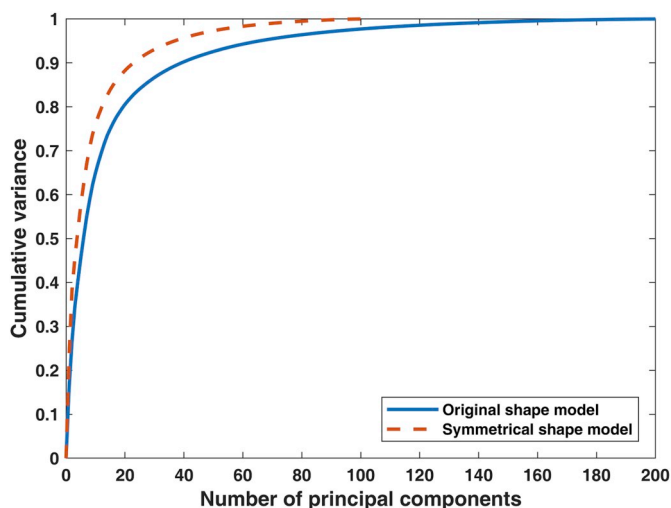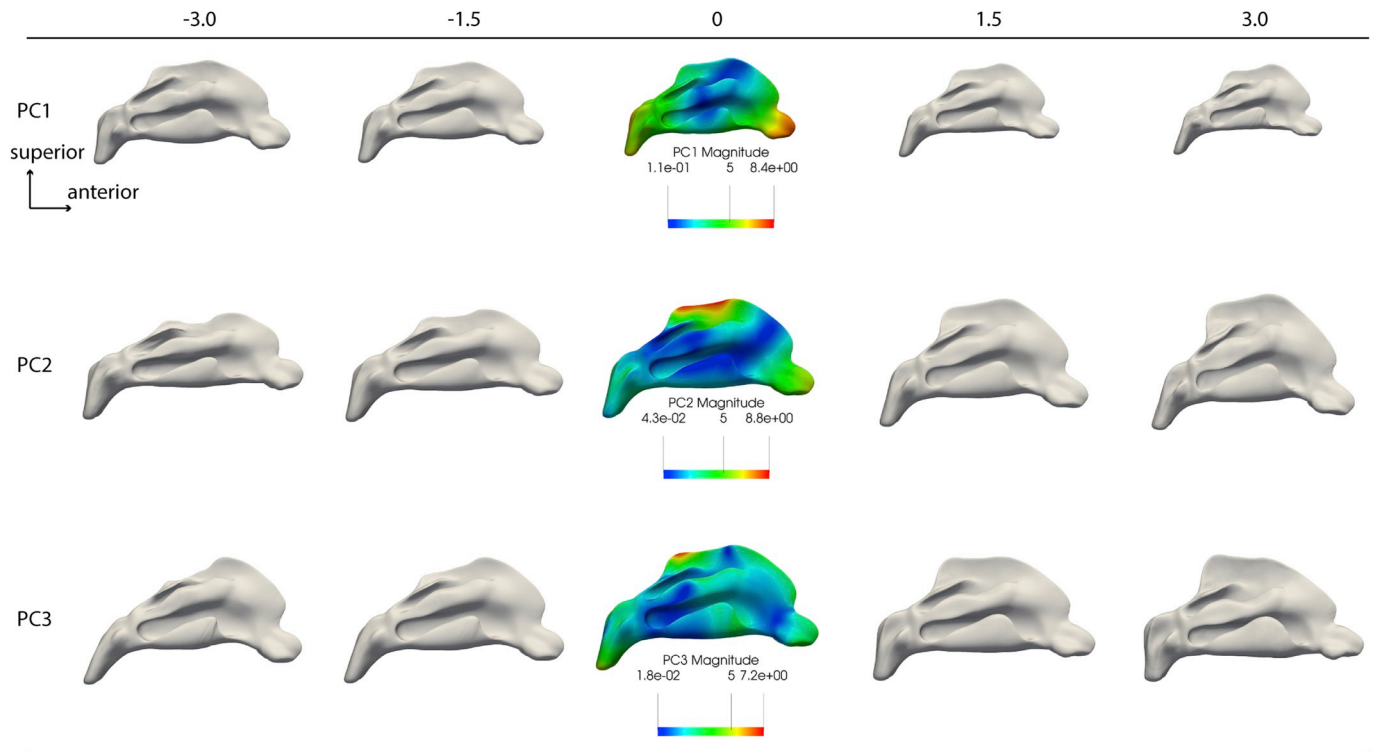
2.2. Computational fluid mechanics

In this paper, steady-state inhalation during breathing at rest was simulated using Reynolds-averaged Navier-Stokes (RANS) equations. For all simulations, we used the commercial software program Star-ccm + v2019.1 (Siemens, Texas, USA), which is based on the finite volume method. Polyhedral mesh elements were used in the bulk of the mesh, and prism layers were used at the boundary. For the thin regions in the nasal cavity, prismatic or pyramid cells were used. A grid independence study was conducted. In our study, the focus was on the global temperature field in the entire nasal cavity, not in any confined region. The cavity with the thinnest regions, being the ninth symmetrical shape mode with a scale factor of 2.4, was examined closely by defining a dense (>400 K) equidistant grid of points throughout the simulation domain. In so doing, we were able to monitor the grid independence of the variable under investigation at the bulk and narrow regions. For the grid resolution that was eventually used (2.6 M elements), the mean relative change was less than 0.13% compared with the result obtained with one resolution level higher (9.9 M elements), which is not proportional to the significant increase in computation time. Grid independence of the velocity was monitored at coronal slices in the nasal cavity. Identical mesh properties were used for all nasal shapes. The exact number of degrees of freedom of the individual nasal shapes depends on the size of the shape and, therefore, varies across the population of shapes. The final grids contained approximately 2.0–3.6 million elements, which are numbers very similar to other studies reported on in the literature (e.g., Ref. [45]). The mesh settings gave a y + value that was much lower than 5, which allowed us to resolve the velocity and thermal boundary layer fully. The lag elliptic blending model, a member of the k - ε family of turbulence models, was applied to model turbulence. The lag elliptic blending model is well suited to model the onset of turbulence. The following velocity and thermal BCs were defined: (1) at the inlets a zero Pa gauge pressure and an air temperature of 5 °C were used, (2) a flow rate of 10 l/min was set, corresponding to breathing at rest [39,46,47] and (3) a no-slip BC and a constant temperature of 32.6 °C [2] were set on the entire wall. All simulations ran on 160 dual-core CPUs (Ivy Bridge).

For the internal flow problem, we defined the flow field using turbulence intensity and a dissipation length scale. The dissipation length scale was determined using the hydraulic diameter specification method. The nose is a complex geometry. However, for breathing at rest, the air velocities are not that high, making the problem a low to medium turbulent case. Therefore, the turbulence intensity was set to 3%, which is slightly higher than the 2.5% used in Ref. [45]. Only a small variation of the hydraulic diameter exists across the population. Consequently, the value for the dissipation length scale calculated at the mean nose was used for the entire population. It was set at a value of 0.08 cm at the inlet and outlet boundaries, only slightly lower than the 0.1 cm used in Ref. [6].

Simulation convergence was based on the residuals of the continuity, momentum, and turbulence quantities. Global engineering values, such as flow rate and pressure drop across the nasal cavity, were also monitored to assess simulation convergence. Fig. 5 shows an example of such a simulation result. The simulation geometry used for this simulation was the mean nose (left) and symmetrical shape mode 1 (right). In this example, the streamlines representing the steady-state solution are color-coded as a function of local airflow velocity.

2.3. Shape generation

All shapes that were used for the analysis were created by applying exactly one eigenmode of the symmetrical or asymmetrical model to the mean shape. Fig. 2 shows that the first 12 principal components represent 69.6% of the total variation captured. Simulations were based on shapes generated using one of these modes. Not every result for which an eigenmode was applied is worth mentioning, and for the sake of

Fig. 2. Cumulative variance as a function of the number of principal components, also known as shape model compactness. For the original shape model (blue solid), the first 12 PCs explain approximately 70% of the total variation present in the population of shapes. The first 20 PCs explain 80%.

Fig. 3. A visual representation of the first three principal components (PCs) of the symmetrical shape model. Each nasal shape is constructed by applying the PC to the mean nasal shape (vector sum) with different values for the scaling factor, depicted in the top row and ranging from 3 standard deviations (std) to −3 std. The color overlay on the mean nose shows which regions are strongly deformed by a PC (deformation magnitude).
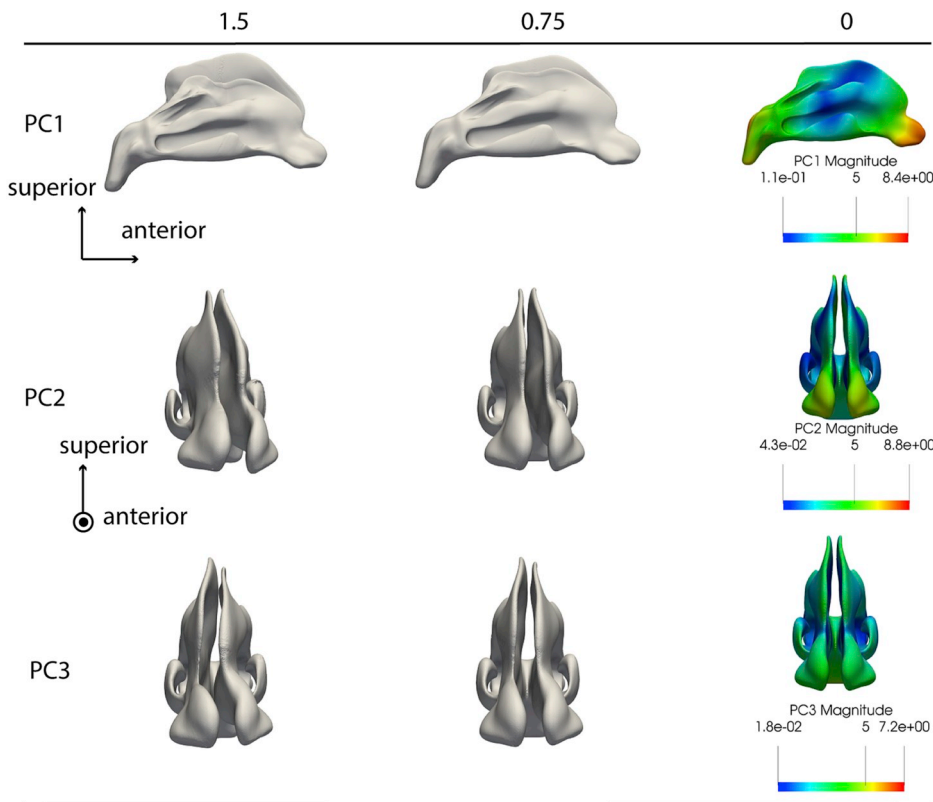
Fig. 4. A visual representation of the first three principal components (PCs) of the asymmetrical shape model. Each nasal shape is constructed by applying the PC to the mean nasal shape (vector sum) with different values for the scaling factor, depicted in the top row and ranging from 1.5 std to 0 std. The color overlay on the mean nose shows which regions are strongly deformed by a PC (deformation magnitude). Shapes for negative values of the scaling factor are not shown because this produces shapes that are the mirrored counterparts of the corresponding positive values.
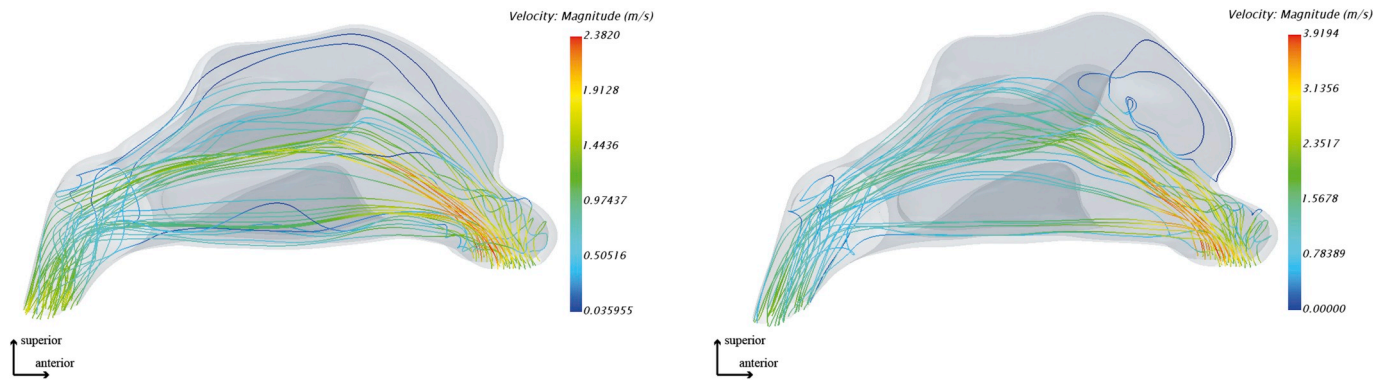
Fig. 5. Two examples of a converged result: (left) for the mean nasal geometry and (right) for the first symmetrical mode. The streamlines, representing the path that massless particles will follow are color-coded with the velocity magnitude. These results will be further discussed in Section 4.

conciseness, these will not be shown in the results. Some of the asymmetrical eigenmodes simulate certain types of nasal septum deviations, as defined by Ref. [48]. The first asymmetrical mode mimics the nasal cycle, showing some clear characteristics: while one air channel shrinks in size, the other channel broadens, and at the same time, the thin region on top, near the olfaction region, grows (caused by a decrease in swelling). The effect of conchae size is studied by using the symmetrical modes. The first eigenmode represents a global non-isotropic size change, toward a smaller or large nasal cavity, depending on the value for the scaling factor in front of the standard deviation (std), with $-3 \leq scale \leq 3$. In the results below, a concise notation is used to represent which principal component is applied and at what scaling factor for the symmetrical and asymmetrical models: $(a)sym_{PC}^{scale}$. For example, $Sym_1^{0.9}$ means that the first principal component of the symmetrical model was applied with a scaling factor of 0.9. When the same principal component is applied multiple times with another scale factor for different figures, the scale factor will be given in the right corner of each figure, and a more general notation will be used: $(a)sym_{PC}$.

3. Results

In this section, we will present the qualitative results provide short descriptions of the important results. For each nasal shape, a volumetric threshold was used for the air temperature. Because of the variation in the literature review of nasopharyngeal temperature discussed in the introduction, we decided to define the threshold at 27 °C. In so doing, the threshold is situated at the lower end of the nasopharyngeal air temperature values. Therefore, it is immediately clear if a nasal shape would have a negative impact on meeting the alveolar condition. Air that has a temperature above 27 °C is transparent, while air with a temperature below or equal to this value is opaque (blue color). This temperature cutoff point enables us to define an isosurface and to asses and compare the heating capacity of different nasal shapes. At the chosen temperature threshold, the range of isosurface size also seems optimal when compared with higher values, which is an additional benefit. Conducting qualitative studies with threshold values that are too low or too high should be avoided since such a practice would lead to large or small isosurfaces respectively for every nasal shape, inhibiting qualitative comparisons. The nasal wall, with its constant temperature of 32.6 °C, is depicted with lower opacity in red.

3.1. The effect of a septum deviation

In this section, the impact of size and shape features related to nasal size are examined using the asymmetrical shape model. The qualitative threshold map for the symmetrical mean nose (Fig. 6, top) forms a reference for subsequent results to be compared with. The effect of different types of septum deviations and their impact on the heating

function of the nose are examined. For asymmetrical Mode 2 and asymmetrical Mode 3, the isosurface reduces in one nasal channel, while the other channel mildly gains size. For asymmetrical Mode 8 (Fig. 7), this gain in size in the opposite channel (left in this case) is not evident. The effect of asymmetrical Mode 10 on isosurface size is smaller compared with the previous modes.

3.2. The effect of size and size-related features

In this section, we investigate the impact of size and shape features related to nasal size using the symmetrical shape model. The effect of symmetrical shape Mode 1 is mainly a scaling of the nasal cavity. However, one distinctive feature exhibited by the mode is the change in the size of the convex region located anteriorly, as shown in Fig. 8 (top). The impact of this feature is examined by scaling the mean nose and comparing the results (Fig. 8, middle) with those of Mode 1. Symmetrical shape Mode 2 is the last mode examined for size-related effects. This mode allows the transformation of the symmetrical mean nose into a narrow, high, and short or a wide, low, and long nasal cavity. An interesting avenue of investigation consists of comparing the results and relating them to literature on the anthropological classification for the external nasal shape and its effect on the conditioning of the air.

3.3. The effect of conchae size

This section examines the effect of conchae size in the absence of asymmetry. Fig. 9 shows the results of Modes 8 and 9, which have a distinct impact on conchae size and the related surface-to-volume ratio.

To conclude this results section, we present results about wall surface area and nasal volume in Fig. 10 using a unitless variable, that is, the normalized surface-to-volume ratio (SVR). The variable is made unitless by taking the square root of S^3 before dividing it by the volume. A subsequent second division (by the unitless SVR of the mean nose) results in a normalized SVR. Moving along the horizontal axis changes the scaling factor of the shape modes.

4. Discussion

4.1. Results

4.1.1. Asymmetrical shape model

In the literature, it is reported that, in a normal nose, the airflow is situated mainly at the floor of the nasal cavity and between the middle meatus and the septum [2,49,50]. Only a fraction of the airflow passes through the meatus and olfactory slit. Although in this paper, the shape model is built from clinical CT scans, the same flow characteristics can be observed, as shown in Fig. 5. Fig. 5 also clearly indicates that the nasal airflow for the mean nose (Fig. 5, left) does not exhibit any flow
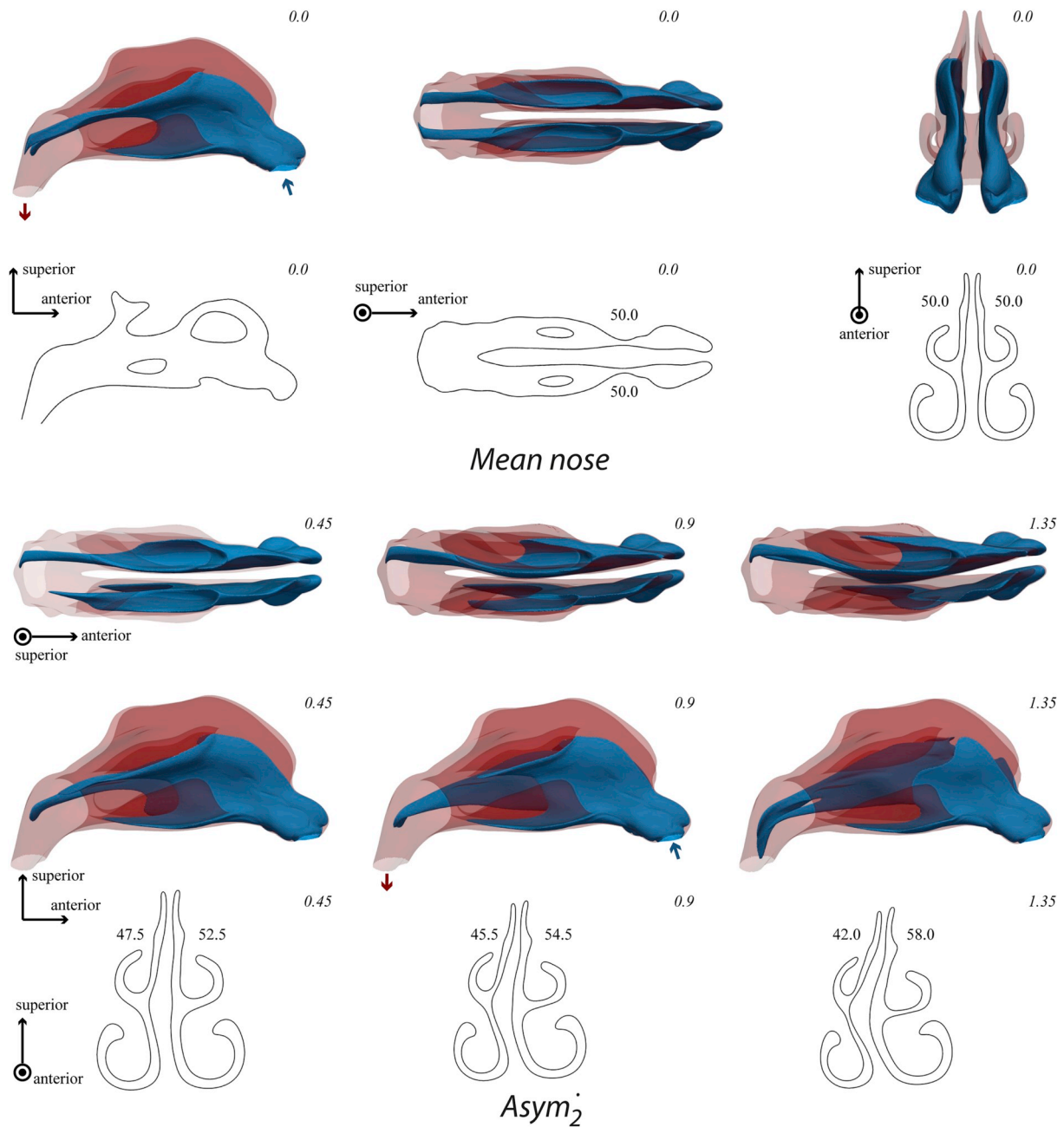
Fig. 6. Qualitative volumetric temperature-threshold maps for the mean nose (top) and the second asymmetrical PC (bottom). Cold air (5 °C) is inhaled. Inhaled air with a temperature above 27 °C is rendered completely transparent. Air with a temperature below 27 °C is shown in blue and opaque. The nasal wall, with its constant temperature of 32.6 °C, is depicted with a lower opacity in red. The numbers in the right top corners for each map provide the scaling factors of the standard deviations. The numbers located at the different coronal, sagittal and transversal slices represent the percentages of the total flow rates passing through the nose. For example, for the mean nose, the 50.0 at both channels indicates that exactly half of the overall flow rate passes through each of both channels, as expected. A coronal slice, located at the plane in which the inferior meatus reaches its maximum height, is shown to clarify the effect of each specific PC.

separation or recirculation, aside from a low number of prominent recirculating streams anteriorly in the nasal vestibule and complex downward-oriented streams posteriorly at the nasopharynx. A similar flow pattern in the nasal cavity was found in previous studies [3,7,8,49, 51]. [52] reported on a region exhibiting clear recirculation that situated downstream of the airway. This region of recirculation extends from the anterior wall and is confined by the anterior region of the middle turbinate. Superiorly, it does not reach the olfactory slit [3]. These characteristics are also clearly visible in the simulation of symmetrical Mode 1 (Fig. 5, right).

In Section 3.1, the asymmetry shape model was used to investigate the effect of asymmetry on heating capacity. More specifically, the

behaviors of certain types of nasal septum deviations were examined. Some of these modes mimic types of septum deviations, as defined by Ref. [48]. The parameterized model makes it possible to go further than a single shape study and, in theory, allows for the continuous examination of the effects of shape deformation.

The second asymmetrical shape mode falls under the category of Type-3 nasal septum deviation (NSD) following the Mladina et al.'s classification. As the second PC, it represents a relatively large part of the variation exhibited by the population of noses used to train the model. Type-3 NSD is also the most frequent NSD encountered [48]. It is clear from Fig. 6 that, in this case, the NSD has its inflection point at the right nasal channel. Comparing the result with the threshold baseline of
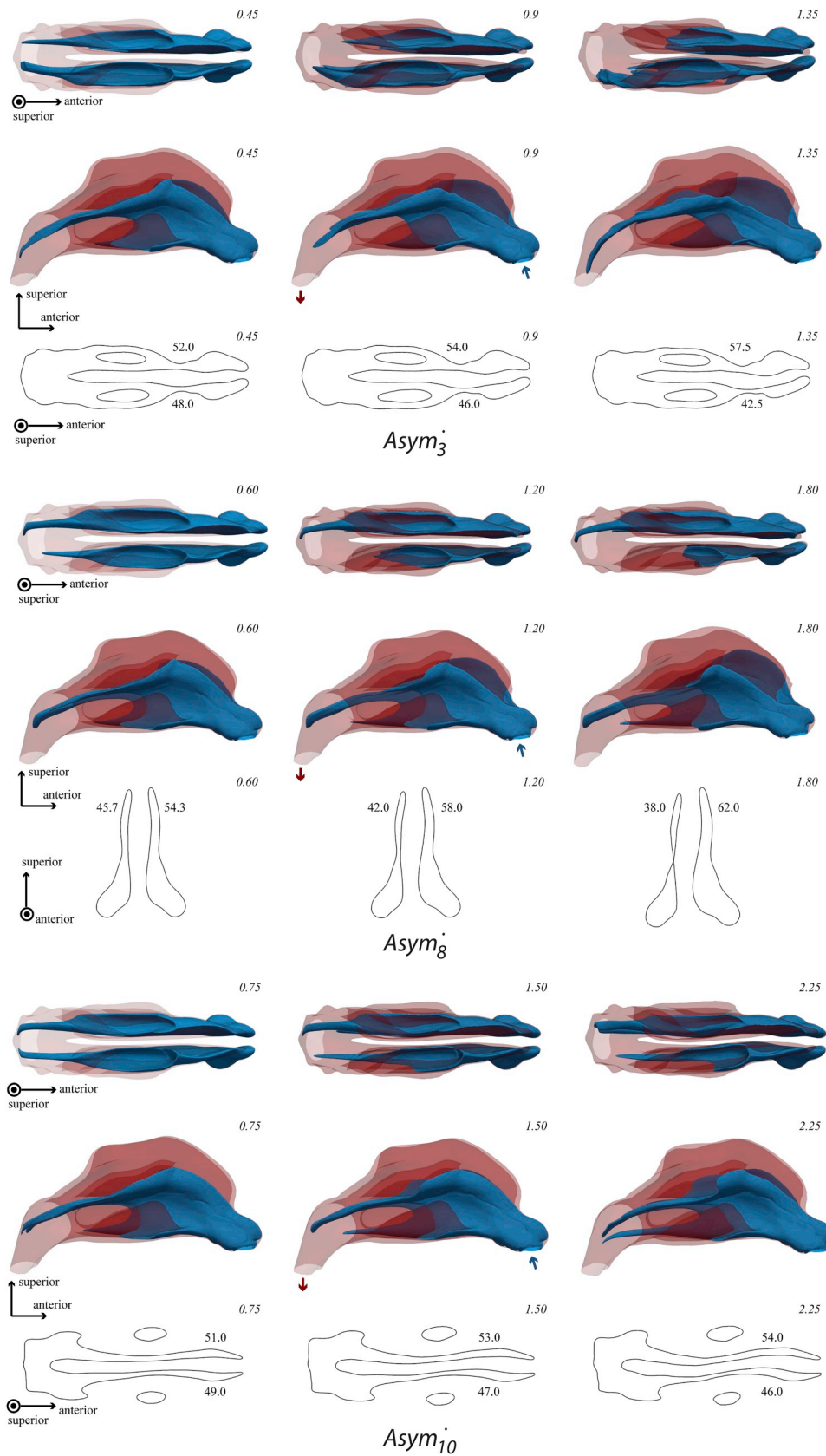
Fig. 7. Qualitative volumetric temperature-threshold maps for asymmetrical PC 3 (top), PC 8 (middle), and PC 10 (bottom). The reader is referred to Fig. 6 for detailed information on the maps.
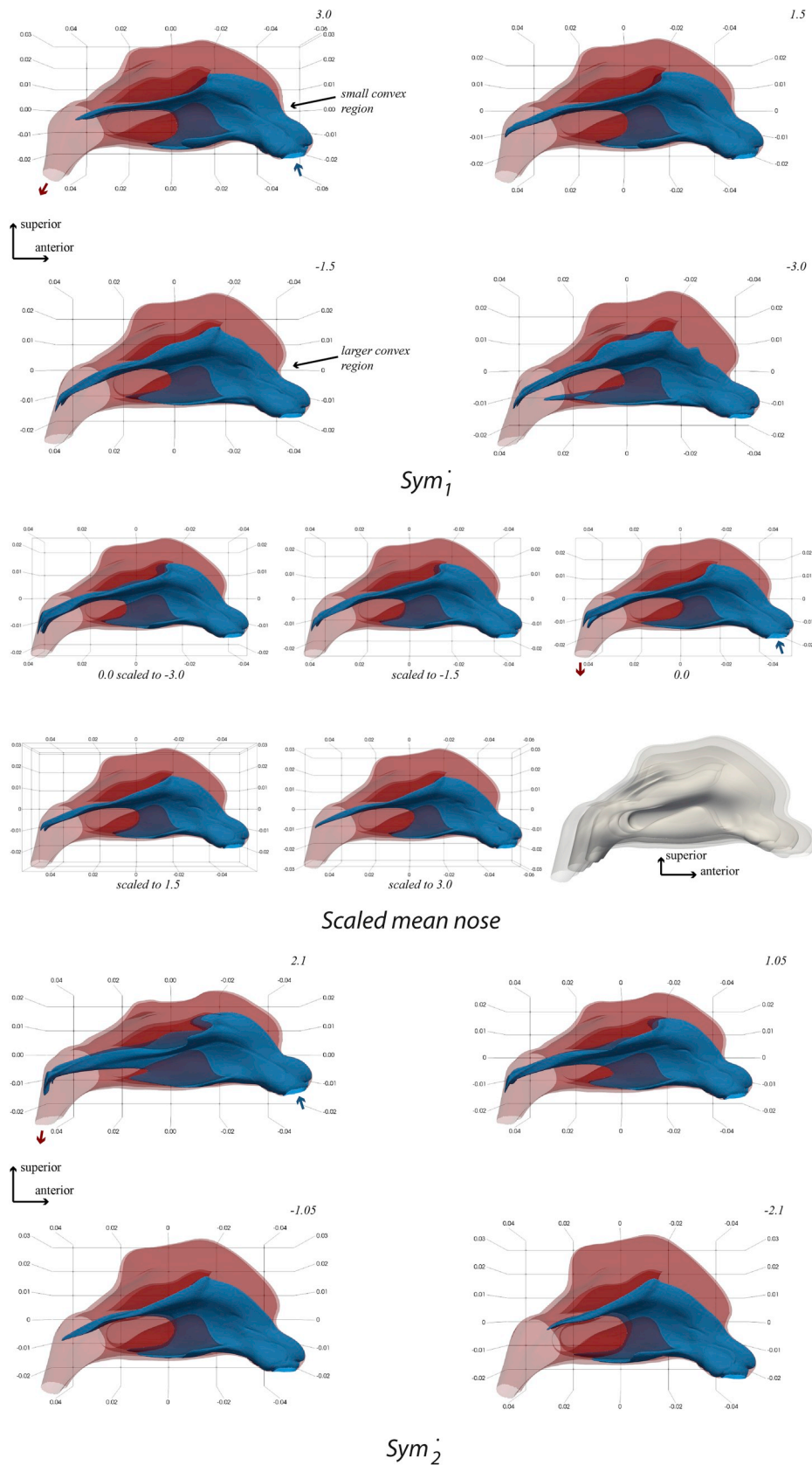
Fig. 8. Qualitative volumetric temperature-threshold maps for symmetrical PC 1 (top), PC 2 (bottom), and the scaled mean nose (middle). See Fig. 6 for detailed information on the maps. Nasal channel flow fraction percentages are no longer shown here because we are dealing with symmetrical shapes. On the right of Fig. 8 (middle), the difference in size for the scaling of the average nose is shown by overlaying the shapes.
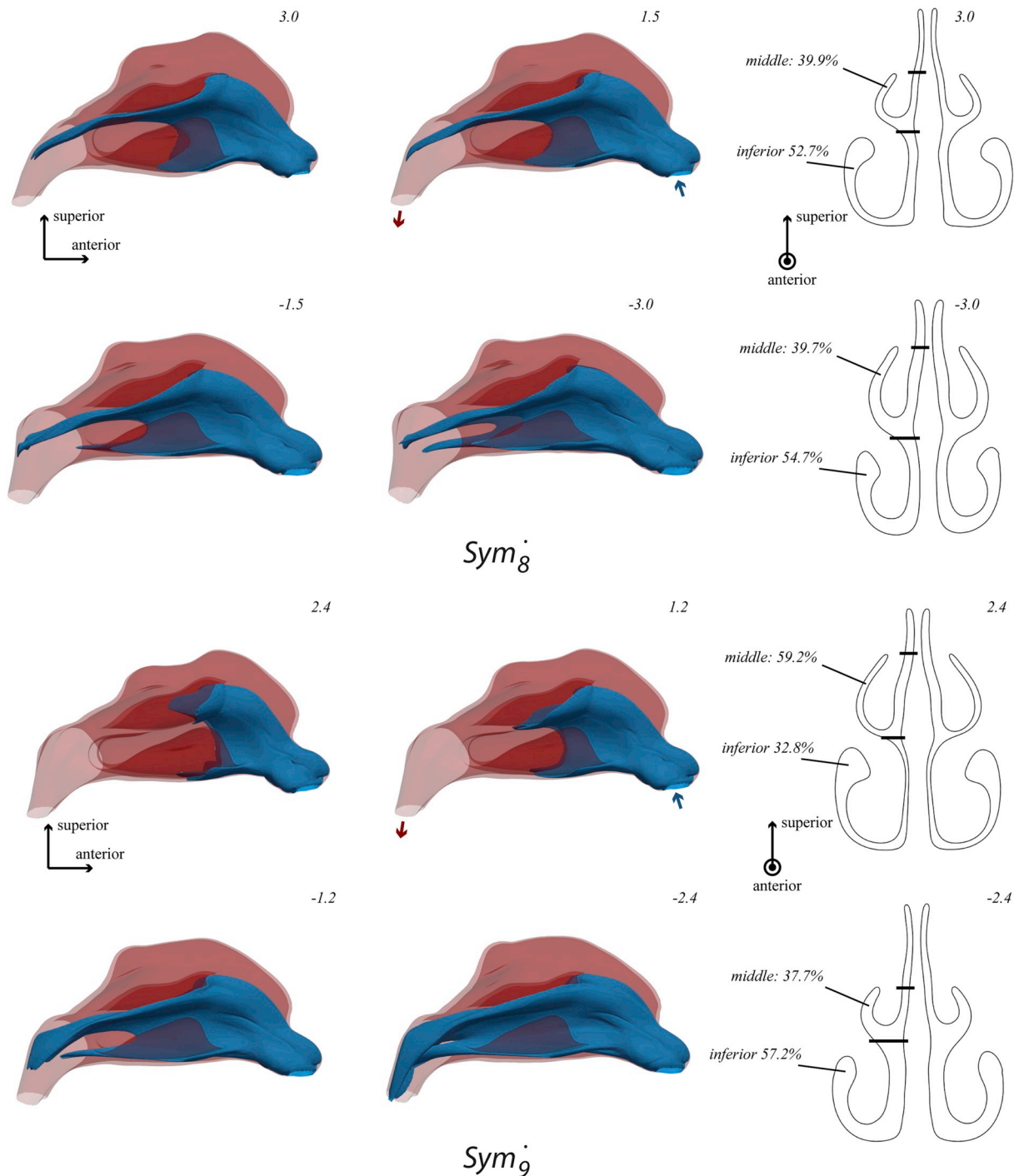
Fig. 9. Qualitative volumetric temperature-threshold maps for symmetrical PC 8 (top), PC 9 (bottom). See Fig. 6, for detailed information on the maps. A coronal slice, located at the plane in which the inferior meatus reaches its maximum height, is shown (right) to clarify the effect of each specific PC. The percentages shown correspond with the fractions of flow rate through the indicated region in one (in this case, the right) nasal channel. The division in regions was carried out manually.

the mean nose, the NSD has a significant impact on the temperature of the air that flows into the post-nasal-region (PNR). Air coming from the right nasal channel reaches the PNR with a higher temperature than before, while the situation is precisely the opposite for the left nasal channel. It is clear from the percentage of total flow rate that an increasing severity of NSD also leads to an increased flow rate in the left nasal channel. Besides the higher flow rate, the SVR in the left nasal channel decreases, while for the right nasal channel, it strongly increases. These results suggest that for patients with a Type-3 NSD and with complaints about the conditioning of cold air, the issue will be

situated in the nasal channel opposite to the inflection point.

The third asymmetrical PC falls under the category of Type-2 NSD. As was the case above, the inflection point of the NSD was at the right side, and the flow rate at this side is negatively correlated with the severity of the NSD. However, despite the increased flow rate in the left channel, the heating capacity improves with increasing severity. Fig. 10 shows the increase in surface-to-volume ratio of the left channel. As a result, the channel is able to condition the air despite the increased flow rate. Following these results, an issue with the conditioning of cold air will be located in the nasal channel at the same side of the inflection
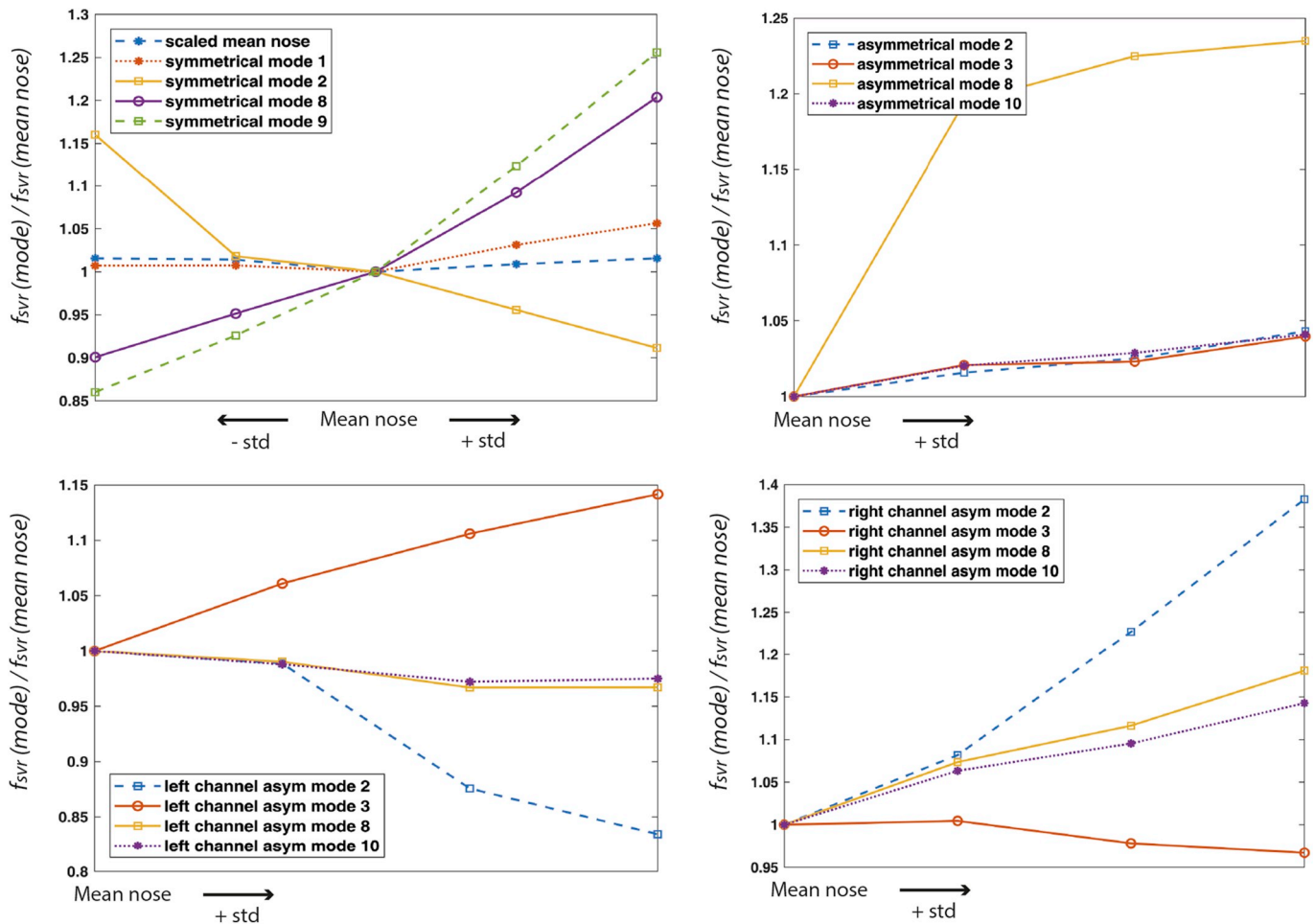
Fig. 10. Normalized unitless surface-to-volume ratio (SVR) on the vertical axis, defined as the square root of S^3 and divided by the volume times the unitless SVR of the mean nose. Moving along the horizontal axis changes the scaling factor of the shape modes. (Top left) SVR for the symmetrical modes. Each line in a graph corresponds with a shape mode, and each data point with one of the shape instances presented in the previous results. Starting from the center (mean nose), the scale factor of the standard deviation (std) decreases or increases respectively. (Top right) SVR for the asymmetrical modes. Only one side on the horizontal axis is shown because of the symmetry for positive and negative std. (Bottom left) SVR for the left nasal channel of the asymmetrical modes. (Bottom right) SVR for the right nasal channel of the asymmetrical modes.

point for patients with a Type-2 NSD.

Mladina's Type-1 NSD describes Mode 8. Once again, it is clear that the NSD influences the flow rate ratio in the channels. However, in this case, the shape deformation has a negligible impact on the heating function of the nose. The left nasal channel perfectly manages the increase in flow rate, despite the small decrease in surface-to-volume ratio, with a negligible change in the volume threshold for air coming from this channel and entering the PNR. The increase in SVR, together with the decrease in flow rate at the right side, has a positive impact on the temperature of the air coming into the PNR. Therefore, the results suggest that patients with a Type-1 NSD, as mimicked by asymmetrical Mode 8, should have no complaints about cold air penetration into the lower airways.

Asymmetrical PC 10 falls under the category of Type-4 NSD, with the recognizable S-shape from the superior view. However, when we look at the results, it seems that this shape deformation does not have a large impact on the heating capacity of the nose, with the largest change being situated in the right nasal channel, which can be explained by the increase in SVR (Fig. 10).

4.1.2. Symmetrical shape model

The symmetrical shape model has been used to investigate the effect of shape changes in the absence of asymmetry. In Section 3.2, the impact of a global size change, a size-related feature exhibited by the shape model, and natural nasal elongation were examined. In Section 3.3, the effects of PCs that have a distinct influence on the size of the conchae were investigated.

Fig. 8 (top) shows the first symmetrical PC. The effect of this PC is non-isotropic scaling that is learned from the natural variation in the clinical nasal population. It is clear from the results that the larger nose has a better heating function than the smaller one when we investigate the threshold volume in the PNR. However, despite the considerable decreases in nasal channel length (approx. 30%) and in nasal height (approx. 22%), as compared with the large nose, the heating function of the small nose does not considerably decrease. One reason could be the larger SVR value for the smaller nose. In general, the heating function of a nose depends not only on the length and the contact area of the nose but also on other variables, such as the amount of turbulence in a nose. However, no evidence for such turbulence was found in the simulation reported on in this paper. Aside from scaling, we can observe that one distinct feature is changed when we investigate in more detail the anterior part of the nose. When the size of the nose shrinks, the anterior inclination point right above the nostrils is pulled in stronger than a general point on the shape, creating a convex region inside the anterior part of the nasal cavity (see Fig. 8, top). This region affects the cross-sectional area of the nasal valve region. For the large nose, this region is much less convex (observed from within). Because this is a feature learned from a population of real noses, one could think this is a natural

and intended restriction to nasal well-functioning. Therefore, we can hypothesize that nasal scaling in the absence of this feature has an impact on the overall functioning of the nasal cavity. In this paper, this phenomenon was investigated for heating by each time scaling the size of the mean nose to that of the shape model instances of Fig. 8 (top), such that, on manual inspection, no size difference is visible. Subsequently, the qualitative threshold maps were calculated. However, when we compared Fig. 8 (middle) with Fig. 8 (top), we were unable to confirm this hypothesis. Consequently, our conclusion is that this size-related feature has no positive impact on the heating of inspired air with flow rates corresponding to breathing at rest. In the future, it would be interesting to investigate the effect of the size of the size-related feature on other nasal functions and for other breathing regimes (e.g., heavy breathing).

In the final part of Section 3.2, the effect of the symmetrical PC 2 on the mean nose was investigated. This PC enabled us to examine the combined effect of width, length, and height. It gradually transforms the mean shape from a wide, low, and long nose (WLL, scale factor = +2.1) into a narrow, high, and shorter nose (NHS, −2.1). From this result, it is clear that the NHS nose is better capable of warming the inhaled cold air, despite being approx. 27% shorter than the WLL nose. This result aligns with what we know about the nasal index. The nasal index is an external nose feature, defined as the ratio of the external width and height. It is used in anthropological studies to classify noses. Three categories exist: (1) leptorrhine (narrow-nosed), (2) mesorrhine (medium-nosed), and (3) platyrrhine (broad-nosed). It has been suggested that these shape differences are related to climate adaption. Broad noses appear in warm and humid climates, where air conditioning is not essential. By contrast, narrow noses appear in cold climates, where the inspired air requires more heating [45]. When we lay these conclusions next to the data in Fig. 10, it is not that surprising that the NHS nose is better able to heat incoming air, compared with the WLL nose. The WLL nose, in general, has a substantially smaller surface-to-volume ratio (SVR) compared with the NHS nose. This shape mode is extracted from real patient data, so all other simultaneous shape deformations are co-related because it is learned from this patient data. Therefore, it can be generalized that an NHS nose is better capable of conditioning incoming air (at least partially) because of a higher SVR specific to these shapes when compared with WLL noses.

In Section 3.3, the effect of conchae size was examined by applying PCs (to the mean nose) that distinctively transform the size of the conchae. In symmetrical PC 8 (Fig. 9, top), the size of the middle conchae (MC) and inferior conchae (IC) are negatively correlated, while for PC 9, they are positively correlated. In symmetrical PC 8, the flow rate in MC and IC stays almost the same during the transformation from 3.0 to −3.0. However, the larger shape of the IC has a clear impact on heating capacity. The size of the MC is larger in the −3.0 case, but at the same time, it is noticeable that the SVR of the middle meatus increases as well. It seems that this simultaneous alteration has a small compounded effect on heating function. For symmetrical Component 9, the impact of enlarged conchae is clear. A smaller volume of the meatus also seems to contribute positively to heating capacity. Both the size of the conchae (contact area) and the volume have an impact on the amount of air coming into contact with the warm boundary, influencing the heating function of the nose. Fig. 10 shows that PC 8 and PC 9 (both shape modes that have a large impact on conchae size without adding any asymmetrical effects) have the largest impact on the surface-to-volume ratio (SVR) compared with the other modes. Related to this large change in SVR, is the large difference in the heating function of the nasal shape, especially evident for PC 9. This strong relation emphasizes the importance of the conchae as a structure for the conditioning of nasal airflow. These outcomes are not new, but the symmetrical nasal shape model approach is. This approach could lead to new insights in the future, beyond what is possible with direct patient data. It was also evident in this study that, in general, for airflow conditions representing breathing at rest, improvement in the nasal heating function concurred with

higher values of the SVR, independent of the presence of (a)symmetry.

Side-to-side comparisons of the anterior and posterior parts of the nasal cavity in Sections 3.2 and 3.3 show that the anterior part is the most effective in the heating of inhaled ambient air. Cold air can be strongly heated by this part alone, as is demonstrated by the result of symmetrical Mode 9. The results also show that, in general, the isosurface reaches the PNR if the air is not heated enough in this anterior part. It suggests that the heating function of inspired air in the posterior part of the nasal cavity is smaller when compared with the anterior part, which confirms the findings of [5]. Another general feature observed throughout the results is that, overall, the inferior turbinate has the strongest contribution to the heating of the inhaled air, which is seen in noses that have a good overall heating function. This result is also found in Refs. [21,23,41].

In the following, the results of the symmetrical modes are compared with the work of [41]; who evaluated the impact of inferior turbinate surgery on the nasal airway heating capacity. They mention that too much reduction of the inferior turbinate can have a negative impact on the heating capacity. In turn, this may result in too low a temperature at the posterior side of the nasal cavity. Chen et al.'s results are in accordance with the results of symmetrical Modes 8 and 9. Mode 8 affects the size of the inferior turbinate, and it is shown that the nasal shape is less capable of heating the airflow at the nasal cavity floor. Mode 9 has a large effect on the size of both the inferior and the middle turbinate. The results show the negative impact on the heating capacity even more clearly [41,53]. also report that one of the main warming zones for the nose is the anterior region around the surface of the inferior turbinate. This finding is in agreement with the results of the results presented here, where the entire inferior turbinates were often completely opaque. However, in our present paper, it is, in general, less straightforward to draw conclusions about the good functioning of the nose or to speak about healthy nasal function. The reason for this is that examined shapes are generated using statistical shape models that are trained using pathological noses (i.e., nasal shapes coming from patients who consulted ENT physicians). When we compare the average temperature in coronal slices defined throughout the nasal cavity with the results in Ref. [41]; the most significant differences are due to the definition of a lower nasal wall temperature (32.6 °C instead of 34 °C) and lower velocity (10 l/min instead of 17.4 l/min). As was the case in Refs. [5,11]; the largest increase in air temperature occurs anteriorly, where after the temperature increments of the inhaled airflow become smaller in relationship to nasal depth.

To the authors' knowledge, literature specifically about the effect of a nasal septum deviation on the heating of inhaled air is still lacking. For this reason, the current study is a good addition to existing literature, but it also makes it harder to draw an in-depth comparison of the results with existing ones. However, studies that provide detailed information about the aerodynamic effects of nasal septal deviations does exist [54]. These studies are strongly related to the nasal heating capacity. They state that the existence of turbulence in the airflow has a destabilizing effect on the boundary layer. Consequently, a larger gradient for heat transfer at the mucosa may exist, which has a positive impact on heat transfer. In general, the results presented in this paper are in accordance with these findings and show that a nasal septum deviation does not necessarily have a detrimental effect on the thermal conditioning of inhaled air. Asymmetrical Mode 3 is an anterior septal deviation [55]. mention that anterior septal deviations tend to shift airflow inferiorly, reducing the airflow in the middle section and causing a reduced mucosal cooling. Comparing the results of Mode 3 with the results of the symmetrical mean nose shows that the air temperature of the flow in the middle section does not increase faster than for the mean nose. In addition, the temperature of the airflow at the floor of the nasal cavity increases somewhat faster for the septum deviation. However, these results do not have to contradict each other. Further detailed investigations (e.g., into turbulence) would be necessary to shed light on these phenomena.

4.2. Approach of this and future work

In this paper, PCA was applied, which resulted in global shape variations. This analysis enabled us to examine the natural variation present in a clinical population and to investigate which effects variations have on the heating function of the nasal cavity. The combination of a symmetrical and asymmetrical shape models allowed us to investigate these effects separately, avoiding having indistinctive results because of compounded effects. Such effects would be there when one uses different surface models directly coming from patients. Another advantage of our study is that the global shape modes are ranked by descending order of shape variation. The order makes it possible to investigate the strongest (magnitude deformation vectors) and the most extensive nasal shape variations, as indicated by the shape model.

The entire nasal wall temperature was set to a constant value in the present study. Despite being an approximation, this is frequently done in heat transport studies [24]. investigated nasal air-conditioning for a constant wall temperature of 37 °C in a model mimicking the nasal cavity. In their study, they underlined the role of the turbinates in the heating process. In a study by Ref. [2]; nasal wall cavity temperature was set to 32.6 °C to study atrophic rhinitis [56]. investigated the effect of virtual surgery on heat transfer in the nasal cavity and also used a constant boundary temperature. As a final example [5], examined the air temperature distribution in the nasal cavity using a constant wall temperature of 34 °C.

Our study presented here lays the foundation to expand the work on both shape models further using time-dependent simulations. Such an approach would allow us to investigate how unsteady effects influence heat exchange and to take into account the spatial and temporal variation of the epithelial temperature during breathing. Because of the existing correspondence between instances created with the shape model, this model is ideally suited for the definition of such a spatially varying wall temperature in an automated manner. The temperature field would have to be defined only once (on the mean nasal shape). Through the existing correspondence, all shape instances would automatically have wall temperature fields defined. Another advantage, demonstrated in Ref. [57]; is that the investigation of surface area, volume and the volume-to-surface ratio of localized anatomical regions in the cavity can also be automatized in the same way as described for the temperature distribution. Aside from this spatial variation of epithelial temperature, another improvement would be the addition of a more complex model that uses a heat flux instead of constant wall temperature. As mentioned above, it is not uncommon to use a constant temperature at the wall in heat transport studies. In our study presented here, it allowed for a straightforward comparison of the different nasal shapes. However, one should be aware that the choice imposes a restriction on the conclusions. In future studies, these conclusions should be further investigated using more complex models.

As a future complementary study, it would be interesting to construct a shape model based on sparse PCA. This model would no longer show any full shapes created from natural variation, but would allow researchers to apply changes to the nasal shape locally, while the other region stays the same. In so doing, there would be no compounded effects, and the impact on nasal functioning of highly localized shape changes could be investigated. Another approach could be to use the current shape model and to identify subspaces (or paths) in the higher dimensional shape space that allowed for variations in the nasal shape without altering the surface area, volume or SVR and to use these subspaces to further investigate the influence of nasal shape variation on the heating function.

Creating a model of healthy patient data would also expand on the study reported here, by allowing us to compare the current data (collected from patients with complaints) with the model and its principal variations built from healthy noses (normative study). Another approach could be to expand the existing training data, making the data set substantially larger and collecting nasal tomographic data from a more diverse population. Dividing this larger set into subgroups based on nasal pathology (cluster analysis) would enable us to investigate and compare the natural variations in shape models separately for each pathological subgroup (comparative study).

5. Conclusion

In this paper, a statistical shape model of the human nasal cavity based on a large clinical training set was built and used to investigate the effects of shape on nasal heating function. It was possible to examine the effect of shape deformation in a quasi-continuous manner using this parameterized model. Through the creation of a symmetrical and an asymmetrical model, influences caused by asymmetry or a lack thereof could be studied separately. In so doing, we were able to avoid compounded shape effects resulting from the comparison of multiple and very different patient-specific shapes.

Ethics

This study was approved by the ethics committee of UZA Hospital, Antwerp, Belgium (registration number: B300201525456) and all data were anonymized.

Declaration of competing interest

None declared.

References

[1] J.S. Rhee, D.T. Book, M. Burzynski, T.L. Smith, Quality of life assessment in nasal airway obstruction, The Laryngoscope 113 (2003) 1118–1122.

[2] G.J. Garcia, N. Bailie, D.A. Martins, J.S. Kimbell, Atrophic rhinitis: a CFD study of air conditioning in the nasal cavity, J. Appl. Physiol. 103 (2007) 1082–1092.

[3] J. Wen, K. Inthavong, J. Tu, S. Wang, Numerical simulations for detailed airflow dynamics in a human nasal cavity, Respir. Physiol. Neurobiol. 161 (2008) 125–135.

[4] M.-Y. Di, Z. Jiang, Z.-Q. Gao, Z. Li, Y.-R. An, W. Lv, Numerical simulation of airflow fields in Two typical nasal structures of empty nose syndrome: a computational fluid dynamics study, PLoS One 8 (2013), e84243.

[5] J. Lindemann, T. Keck, K.M. Wiesmiller, B. Sander, H.-J. Brambs, G. Rettinger, D. Pless, A numerical simulation of intranasal air temperature during inspiration, The Laryngoscope 114 (2004) 1037–1041.

[6] X.B. Chen, H.P. Lee, V.K.H. Chong, D.Y. Wang, A computational fluid dynamics model for drug delivery in a nasal cavity with inferior turbinate hypertrophy, J. Aerosol Med. Pulm. Drug Deliv. 23 (2010) 329–338.

[7] K. Keyhani, P.W. Scherer, M.M. Mozell, Numerical simulation of airflow in the human nasal cavity, J. Biomech. Eng. 117 (1995) 429–441.

[8] R.P. Subramaniam, R.B. Richardson, K.T. Morgan, J.S. Kimbell, R.A. Guilmette, Computational fluid dynamics simulations of inspiratory airflow in the human nose and nasopharynx, Inhal. Toxicol. 10 (1998) 91–120.

[9] O. Grant, N. Bailie, J. Watterson, J. Cole, G. Gallagher, B. Hanna, Numerical model of a nasal septal perforation, Stud. Health Technol. Inform. 107 (2004) 1352–1356.

[10] D.J. Doorly, D.J. Taylor, R.C. Schroter, Mechanics of airflow in the human nasal airways, Respir. Physiol. Neurobiol. 163 (2008) 100–110.

[11] S.C. Leong, X.B. Chen, H.P. Lee, D.Y. Wang, A review of the implications of computational fluid dynamic studies on nasal airflow and physiology, Rhinology 48 (2010) 139–145.

[12] D.O. Frank-Ito, J.S. Kimbell, P. Laud, G.J. Garcia, J.S. Rhee, Predicting postsurgery nasal physiology with computational modeling: current challenges and limitations, Otolaryngol. Head Neck Surg. 151 (2014) 751–759.

[13] K. Inthavong, J. Ma, Y. Shang, J. Dong, A.S.R. Chetty, J. Tu, D. Frank-Ito, Geometry and airflow dynamics analysis in the nasal cavity during inhalation, Clin. Biomech. 66 (June 2019) 97–106.

[14] R.S. Bailey, K.P. Casey, S.S. Pawar, G.J.M. Garcia, Correlation of nasal mucosal temperature with subjective nasal patency in healthy individuals, JAMA Facial Plast. Surg. 19 (2017) 46–52.

[15] K. Zhao, J. Jiang, K. Blacker, B. Lyman, P. Dalton, B.J. Cowart, E.A. Pribitkin, Regional peak mucosal cooling predicts the perception of nasal patency, The Laryngoscope 124 (2013) 589–595.

[16] C.D. Sullivan, G.J. Garcia, D.O. Frank-Ito, J.S. Kimbell, J.S. Rhee, Perception of better nasal patency correlates with increased mucosal cooling after surgery for nasal obstruction, Otolaryngology-Head Neck Surg. 150 (2014) 139–147.

[17] M.L. Noback, K. Harvati, F. Spoor, Climate-related variation of the human nasal cavity, Am. J. Phys. Anthropol. 145 (2011) 599–614.

[18] A.A. Zaidi, B.C. Mattern, P. Claes, B. McEcoy, C. Hughes, M.D. Shriver, Investigating the case of human nose shape and climate adaptation, PLoS Genet. 13 (2017), e1006616.

[19] A. Thomson, L.H.D. Buxton, Man's nasal index in relation to certain climatic conditions, J. R. Anthropol. Inst. 53 (1923) 92–122.

[20] S.C. Leong, R. Eccles, A systematic review of the nasal index and the significance of the shape and size of the nose in rhinology, Clin. Otolaryngol. 34 (2009) 191–198.

[21] J. Lindemann, H.J. Brambs, T. Keck, K.M. Wiesmiller, G. Rettinger, D. Pless, Numerical simulation of intranasal airflow after radical sinus surgery, Am. J. Otolaryngol. 26 (2005) 175–180.

[22] S. Naftali, R.C. Schroter, R.J. Shiner, D. Elad, Transport phenomena in the human nasal cavity: a computational model, Ann. Biomed. Eng. 26 (1998) 831–839.

[23] D. Pless, T. Keck, K. Wiesmiller, G. Rettinger, A.J. Aschoff, T.R. Fleiter, J. Lindemann, Numerical simulation of air temperature and airflow patterns in the human nose during expiration, Clin. Otolaryngol. 29 (2004) 642–647.

[24] S. Naftali, M. Rosenfeld, M. Wolf, D. Elad, The air-conditioning capacity of the human nose, Ann. Biomed. Eng. 33 (2005) 545–553.

[25] D. Pless, T. Keck, K.M. Wiesmiller, R. Lamche, A.J. Aschoff, J. Lindemann, Numerical simulation of airflow patterns and air temperature distribution during inspiration in a nose model with septal perforation, Am. J. Rhinol. 18 (2004) 357–362.

[26] V. Goodarzi-Ardakani, M. Taeibi-Rahni, M.R. Salimi, G. Ahmadi, Computational simulation of temperature and velocity distribution in human upper respiratory airway during inhalation of hot air, Respir. Physiol. Neurobiol. 223 (2016) 49–58.

[27] M.A. Burgos, E. Sanmiguel-Rojas, A. Martín-Alcántara, M. Hidalgo-Martínez, Effects of the ambient temperature on the airflow across a Caucasian nasal cavity, Int. J. Numer. Methods Biomed. Eng. 30 (2014) 430–445.

[28] J.-H. Lee, Y. Na, S.-K. Kim, S.-K. Chung, Unsteady flow characteristics through a human nasal airway, Respir. Physiol. Neurobiol. 172 (2010) 136–146.

[29] D.-W. Kim, S.-K. Chung, Y. Na, Numerical study on the air conditioning characteristics of the human nasal cavity, Comput. Biol. Med. 86 (2017) 18–30.

[30] D. Elad, M. Wolf, T. Keck, Air-conditioning in the human nasal cavity, Respir. Physiol. Neurobiol. 163 (2008) 121–127.

[31] T. Keck, J. Lindemann, Numerical simulation and nasal air-conditioning, GMS Curr. Top. Otorhinolaryngol., Head Neck Surg. 9 (2010) Doc08.

[32] S. Ingelstedt, B. Ivstam, Study on the humidifying capacity of the nose, Acta Otolaryngol. 49 (1951) 286–290.

[33] P. Cole, Some aspects of temperature, moisture and heat relationships in the upper respiratory tract, J. Laryngol. Otol. 67 (1953) 449–456.

[34] E.R. McFadden, B.M. Pichurko, H.F. Bowman, E. Ingenito, S. Burns, N. Dowling, J. Solway, Thermal mapping of the airways in humans, J. Appl. Physiol. 58 (1985) 564–570.

[35] F.P. Primiano Jr., G.M. Saidel, F.W. Montague, K.L. Kruse, C.G. Green, J.G. Horowitz, Water vapour and temperature dynamics in the upper airways of normal and CF subjects, Eur. Respir. J. 1 (1988) 407–414.

[36] R.D. Farley, K.R. Patel, Comparison of air warming in the human airway with a thermodynamic model, Med. Biol. Eng. Comput. 26 (1988) 628–632.

[37] P. Rouadi, F.M. Baroody, D. Abbott, E. Naureckas, J. Solway, R.M. Nacleiro, A technique to measure the ability of the human nose to warm and humidify air, J. Appl. Physiol. 87 (1999) 400–406.

[38] W. Oczenski, H. Andel, A. Werba, Atmen - Atemhilfen. Thieme, Stuttgart, 2003, ISBN 3-13-137696-1, p. 274.

[39] B.M. Hariri, J.S. Rhee, G.J. Garcia, Identifying patients who may benefit from inferior turbinate reduction using computer simulations, The Laryngoscope 125 (2015) 2635–2641.

[40] G.J.M. Garcia, J.S. Rhee, B.A. Senior, J.S. Kimbell, Septal deviation and nasal resistance: an investigation using virtual surgery and computational fluid dynamics, Am. J. Rhinol. Allergy 24 (2010) e46–e53.

[41] X.B. Chen, H.P. Lee, V.F.H. Chong, D.Y. Wang, Numerical simulation of the effects of inferior turbinate surgery on nasal airway heating capacity, Am. J. Rhinol. Allergy 24 (2010) e118–e122.

[42] J. Lindemann, T. Keck, K.M. Wiesmiller, G. Rettinger, H.J. Brambs, D. Pless, Numerical simulation of intranasal air flow and temperature after resection of the turbinates, Rhinology 43 (2005) 24–28.

[43] W.E. Lorensen, H.E. Cline, Marching cubes: a high resolution 3D surface construction algorithm, ACM SIGGRAPH Comput. Graph. 21 (1987) 163–169.

[44] T. Huysmans, J. Sijbers, B. Verdonk, Automatic construction of correspondences for tubular surfaces, IEEE Trans. Pattern Anal. Mach. Intell. 32 (2010) 636–651.

[45] K. Zhao, J. Jiang, What is normal nasal airflow? A computational study of 22 healthy adults, Int. Forum Allergy Rhinol. 4 (2014) 435–446.

[46] ICRP, Human Respiratory Tract Model for Radiological Protection, Elsevier, New York, 1994.

[47] J.H. Zhu, H.P. Lee, K.M. Lim, S.J. Lee, D.Y. Wang, Evaluation and comparison of nasal airway flow patterns among three subjects from Caucasian, Chinese and Indian ethnic groups using computational fluid dynamics simulation, Respir. Physiol. Neurobiol. 175 (2011) 62–69.

[48] R. Mladina, E. Čujić, M. Šubarić, K. Vuković, Nasal septal deformities in ear, nose, and throat patients: an international study, Am. J. Otolaryngol. 29 (2008) 75–82.

[49] J.T. Kelly, A.K. Prasad, A.S. Wexler, Detailed flow patterns in the nasal cavity, J. Appl. Physiol. 89 (2000) 323–337.

[50] M. Wolf, S. Naftali, R.C. Schroter, D. Elad, Air-conditioning characteristics of the human nose, J. Laryngol. Otol. 118 (2004) 87–92.

[51] K. Zhao, P.W. Scherer, S.H. Hajiloo, P. Dalton, Effect of anatomy on human nasal air flow and odorant transport patterns: implications for olfaction, Chem. Senses 29 (2004) 365–379.

[52] K. Keyhani, P.W. Scherer, M.M. Mozell, A numerical model of nasal odorant transport for the analysis of human olfaction, J. Theor. Biol. 186 (1997) 279–301.

[53] J. Lindemann, T. Keck, K. Wiesmiller, B. Sander, H.-J. Brambs, G. Rettinger, D. Pless, Nasal air temperature and airflow during respiration in numerical simulation based on multislice computed tomography scan, Am. J. Rhinol. 20 (2006) 219–223.

[54] X.B. Chen, H.P. Lee, V.F. Chong, de Y. Wang, Assessment of septal deviation effects on nasal air flow: a computational fluid dynamics model, The Laryngoscope 119 (2009) 1730–1736.

[55] K.P. Casey, A.A.T. Borojeni, L.J. Koenig, J.S. Rhee, G.J.M. Garcia, Correlation between subjective nasal patency and intranasal airflow distribution, Otolaryngol. Head Neck Surg. 156 (2017) 741–750.

[56] J.S. Kimbell, D.O. Frank, P. Laud, G.J.M. Garcia, J.S. Rhee, Changes in nasal airflow and heat transfer correlate with symptom improvement after surgery for nasal obstruction, J. Biomech. 46 (2013) 2634–2643.

[57] W. Keustermans, T. Huysmans, F. Danckaers, A. Zarowski, B. Schmelzer, J. Sijbers, J.J.J. Dirckx, High quality statistical shape modelling of the human nasal cavity and applications, R. Soc. Open Sci. 5 (2018) 181558.